Molecular-Weight Dependence of Enthalpy Relaxation of PMMA

Laura Andreozzi,* Massimo Faetti, Marco Giordano, and Fabio Zulli

Physics Department of the University of Pisa and I.N.F.M U.d.R. Pisa, Largo Pontecorvo 3, I-56127 Pisa, Italy

Received April 5, 2005; Revised Manuscript Received May 17, 2005

ABSTRACT: The effects of the molecular weight on the physical aging of polymers were investigated by means of differential scanning calorimetry (DSC) experiments in five PMMA samples with mass values across the entanglement mass M_e. The Tool−Narayanaswamy−Moynihan (TNM) model and a recent configurational entropy approach were systematically compared with the experiments. For the samples with the lowest molecular weights, the two approaches exhibited similar agreement with experiments; however, in the systems with higher molecular weights, the TNM model met major difficulties, and a clear improvement was obtained with the other model. The additional parameter introduced by the entropic model showed a strong molecular-weight dependence, with a sharp increase at the entanglements mass of PMMA. These results evidence the role of the chain entanglements on the physical aging of polymers. Finally, the influence of the molecular weight on the fragility was investigated and related to the recent literature debates on this topic.

1. Introduction

It is known that the structural relaxation, or physical aging, of polymers and glass-formers depends on the kinetic character of the glass-transition phenomenon. In particular, when a glass-former is cooled from an equilibrium state, its molecular mobility strongly decreases until the system is no more able to follow, in thermodynamic equilibrium, the temperature changes, so that the glassy state sets in.[1] Then, if a glassy material is kept isothermically below its glass-transition temperature, it slowly relaxes, attempting to restore the equilibrium thermodynamics.

Several phenomenological and molecular approaches have been proposed to describe the structural relaxation of glasses,[2−10] but a universal model is still lacking. The enthalpy relaxation of glasses is usually described with models developed in the framework of the Tool−Narayanaswamy−Moynhian (TNM) theory of the glass transition.[2−5,7] These approaches provide a qualitative reproduction of all the main features of the enthalpy aging processes, which can be detected suitably by performing differential scanning calorimetry (DSC) experiments.[7]

However, severe discrepancies between theory and experiments have been observed, especially in polymers, when curves obtained under different conditions were compared.[7,11,12] Problems, therefore, can arise in connection with the physical meaning of the model parameters, which should be material parameters independent of the thermal history of the sample,[11−13] and with the predictions of the limit asymptotic values of the enthalpy lost on aging the polymeric glasses.[14−16] For these reasons, extensions and modifications of the TNM model have been proposed.[13,17−20] In this respect, it is worth noting that TNM model was first developed, taking into account experimental data from low-molecular-weight inorganic glasses,[3,4] and the implicit assumption that polymers behave in a similar way could be questionable. In fact, the properties and dynamics of polymer melts exhibit marked variations with the molecular mass, which can be suitably described by the Rouse theory in unentangled chains[21] (low masses) and the reptation model[21,22] in entangled polymers (high masses).

The existence of topological constraints, such as chain entanglements, is completely ignored in the TNM-based models. Different researchers suggested that some of the observed difficulties with high-mass polymers might be related to some missing information[23,24] on the segmental dynamics and conformational rearrangements of the polymer main chain that control the structural relaxation of the polymers.

Interestingly enough, some effects of the entanglements on the aging mechanism of polymers have been recently highlighted in different systems with the use of special drying methods[25−27] that provide highly disentangled systems. Indeed, after annealing the samples in the glass, the enthalpy recovery measured by DSC thermograms, showed a quite different behavior for the disentangled systems with respect to the entangled ones.

The aim of this work is a detailed study on the predictive power of TNM formalism and of a recent entropic approach[18−20] (GR model) where an additional parameter is introduced, possibly mimicking the effects of chain entanglements.

The study is carried out by performing DSC experiments in a series of poly(methyl methacrylates) (PMMA), whose molecular weights range across the PMMA entanglement mass, the latter being a signature of the onset of the entangled dynamics.

In the next section, the TNM formalism is briefly described and the difficulties encountered in applying it to polymers are discussed more in detail. The GR approach is also presented.

2. Theory

The TNM theory is based on some fundamental assumptions[7] intimately related to the peculiar nature of the glassy state. To consider the nonexponential character of relaxation in glass-forming systems, the

* Author to whom correspondence should be addressed: e-mail laura.andreozzi@mail.df.unipi.it.

10.1021/ma0507037 CCC: $30.25
Published on Web 06/18/2005

stretched exponential function:

$$\Phi(t) = \exp\left[-\left(\frac{t}{\tau}\right)^{\beta}\right] \quad (1)$$

is used as a relaxation function, where the shape parameter β is considered constant by invoking the time−temperature superposition principle.[28] A second basic feature of the structural relaxation of glasses is its nonlinear character attributable to the out-of-equilibrium nature of the glassy state. During the aging, the structure of the system changes, providing a self-retarding relaxation mechanism. This peculiar feature is introduced in the TNM model by assuming that the instantaneous relaxation time depends on both temperature and structure. The fictive temperature T_f,[29] defined through the relation:

$$H(T) = H_{eq}(T_f) - \int_T^{T_f} C_p^{glass}(\theta)\, d\theta \quad (2)$$

provides the structural parameter to the model.

In eq 2, $H_{eq}(T_f)$ is the equilibrium value of enthalpy at temperature T_f, whereas $C_p^{glass}(T)$ is the unrelaxed glassy heat capacity of the system. A key feature of this definition is the implicit assumption that the equilibrium values of the thermodynamic variables in the glassy state are obtained by extrapolating the equilibrium liquid or rubbery curves below T_g ($dH_{eq}(T)/dT \equiv C_p^{liq}(T)$). The model then assumes that linearity can be restored through the definition of a reduced time $\xi(t) = \int dt/\tau(T(t), T_f(t))$, so that the Boltzmann superposition principle can be used to obtain the structural changes during cooling/heating procedures:[4]

$$T_f(T) = T_0 + \int_{T_0}^{T} dT'\left\{1 - \exp\left(-\left[\int_{T'}^{T} \frac{dT''}{Q\tau(T_f,T'')}\right]^{\beta}\right)\right\} \quad (3)$$

In eq 3, T_0 is a reference temperature well above T_g and $Q = Q_{c,h}$ is the cooling/heating rate. In a typical DSC experiment, an annealing step at $T_a < T_g$ for a period t_a is performed after the first cooling from equilibrium; in such a case, a term of the form:

$$\int_0^{t_a} \frac{dt'}{\tau(T_f(t'), T_a)}$$

has to be added in the reduced time calculus (the second integration in eq 3). By numerical integration of eq 3, the evolution of the fictive temperature can be evaluated. The results are usually presented as normalized heat capacity curves (dT_f/dT), to be compared with the correspondent experimental data obtained by differentiating eq 2:

$$\frac{dT_f}{dT} = \frac{(C_p(T) - C_p^{glass}(T))}{\Delta C_p(T_f)} \approx \frac{(C_p(T) - C_p^{glass}(T))}{\Delta C_p(T)} \equiv C_p^{N}(T) \quad (4)$$

In the equation, $\Delta C_p(T) = C_p^{liq}(T) - C_p^{glass}(T)$ is the heat capacity difference between the glassy and liquid state.

Several expressions were proposed relating instantaneous relaxation times, temperature, and fictive temperature.[7] The most known ones are the phenomenological Narayanaswamy−Moynihan (NM)[2−4] equation and the Scherer−Hodge (SH)[5,24] one

$$\tau(T_f, T) = A \exp\left\{\frac{x\Delta h}{RT} + \frac{(1-x)\Delta h}{RT_f}\right\} \quad \text{NM} \quad (5)$$

$$\tau(T_f, T) = A \exp\left\{\frac{B}{RT(1 - T_2/T_f)}\right\} \quad \text{SH} \quad (6)$$

Because of the additional assumptions needed to obtain the SH expression by extending the Adam-Gibbs theory[30] to the out-of-equilibrium case, the formalism described here is usually referred to as AGV (Adam−Gibbs−Vogel) model when the SH relation is assumed. Even if the SH equation is physically more consistent than the NM one, because it recovers the Vogel−Fulcher temperature dependence of the equilibrium relaxation times, the two equations are very similar as far as the predictive power is concerned, at least for experiments not too far from the thermodynamic equilibrium.[7,31] It is important to remark that a key feature of this approach is that the parameters (A, x, Δh, β or A, B, T_2, β) are material parameters. Consequently, they should be able to describe all the possible experiments, independently of the specific thermal history adopted.

Examples can be found in the literature where the TNM approach describes the enthalpy relaxation in low-molecular-weight glass-forming systems fairly well,[3,4,32−34] whereas major discrepancies have been observed in several polymeric systems.[11,12,17,35,36] The most important difficulties concern the strong dependence of the model parameters on the thermal history and the overestimation of the enthalpy lost on aging the samples for long periods of time.

The first flaw has been often attributed to experimental errors such as thermal lag. However, in a recent paper,[37] thermal gradients were included somehow in the model calculations, but the discrepancies persisted. Furthermore, incompatibilities among different thermograms were also evidenced at very low heating rates.[38]

Other possibilities for the model failure can be taken back to the assumed thermorheological simplicity, which could be questioned. Also, the treatment adopted for nonlinearity has been recently criticized.[39] These topics cannot be ruled out and could be truly responsible for some of the observed deviations.

A different explanation that could reconcile to the same ground the two main problems, not independence of model parameters and overestimation of the enthalpy loss, is related to the use of fictive temperature and then to the true possibility of associating an equilibrium state to an out-of-equilibrium condition.

According to the definition of the fictive temperature, it is obtained that the maximum amount of enthalpy releasable at a given temperature, $T_a < T_g$, may be approximately evaluated by the expression:[7,40]

$$\Delta H_\infty(T_a) \approx \Delta C_p(T_g)(T_g - T_a) \quad (7)$$

Adopting the enthalpic definition of T_g,[41] this relation should provide an approximation by defect of the experimental $\Delta H_\infty(T_a)$.[40] Instead, several studies can be found in the literature,[12,14−18] where eq 7 provided a clear overestimation of the experimental $\Delta H_\infty(T_a)$ in polymers. In this respect, it should be pointed out that a realistic experimental estimation of $\Delta H_\infty(T_a)$ is possible only in a very narrow temperature interval around

T_g, whereas alternative approaches on the basis of empirical procedures[12,15] are questionable.

However, these findings could depend on the failure of the excess of thermodynamic variables in approaching the zero value at long times. It implies that the extrapolation of the melt behavior does not provide the limit values of the thermodynamic observables in the glass as assumed in the definition of fictive temperature. Then, a possible role of chain entanglements could be invoked.

In this respect, it is worth noting that a recently developed configurational entropy approach,[18−20] which defines the state at long times of the structural relaxation process by adding a parameter, was found to improve the agreement with the experiments in several polymers, provided that the limit state was intermediate between the out-of-equilibrium initial state and the extrapolated equilibrium state.[17−20,42] In this approach, the configurational entropy S_c was directly used as a structural parameter without resorting to the fictive temperature concept. An evolution equation was proposed that is in form very similar to the constitutive equation of the TNM model:

$$S_c(t) = S_c^{eq}(T_0) + \int_{T_0}^{T(t)} \frac{\Delta C_p^{lim}(\theta)}{\theta} d\theta - \sum_{i=1}^{n} \left(\int_{T_{i-1}}^{T_i} \frac{\Delta C_p^{lim}(\theta)}{\theta} d\theta \right) \cdot \exp\left\{ -\left(\int_{t_{i-1}}^{t_i} \frac{d\lambda}{\tau(\lambda)} \right)^{\beta} \right\} \quad (8)$$

where the equilibrium configurational entropy is defined as usual:

$$S_c^{eq}(T) = \int_{T_2}^{T} \frac{\Delta C_p(\theta)}{\theta} d\theta \quad (9)$$

In this equation, T_2 plays the role of the Kauzmann temperature.[43] As for the AGV model, the out-of-equilibrium relaxation times are defined by extending the Adam−Gibbs theory:

$$\tau(t) = \tau(S_c(t), T(t)) = A \exp\left(\frac{B}{S_c T}\right) \quad (10)$$

The difference between this approach and the AGV model is mainly due to the fact that, in eq 8, the term $\Delta C_p^{lim}(T) = C_p^{lim}(T) - C_p^{glass}(T)$ appears instead of $\Delta C_p(T)$, expected in principle. In other words, the assumption that the limit value of configurational heat capacity in the glass (and then entropy and enthalpy) is obtained by the extrapolation procedure from the melt ($C_p^{lim}(T) = C_p^{liq}(T)$ for $T < T_g$) is no more needed and other possibilities can be tested. Finally, an identical relaxation mechanism for configurational entropy and enthalpy is assumed:

$$H_c(T) = H_c^{lim}(T) - \sum_{i=1}^{n} \left(\int_{T_{i-1}}^{T_i} \Delta C_p^{lim}(\theta) d\theta \right) \cdot \exp\left\{ -\left(\int_{t_{i-1}}^{t_i} \frac{d\lambda}{\tau(\lambda)} \right)^{\beta} \right\} \quad (11)$$

so that the theoretical $C_p(T)$ curves can be obtained from the relationship:

$$C_p(T) - C_p^{glass}(T) = \frac{\partial H_c}{\partial T} \quad (12)$$

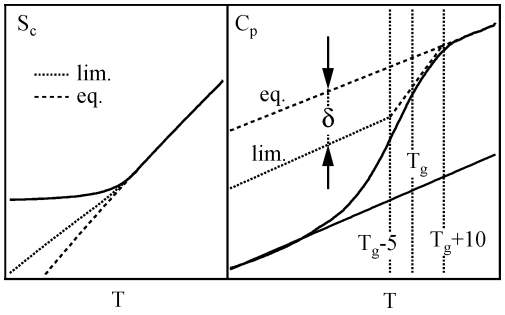

Figure 1. Definition of the phenomenological parameter δ introduced in the configurational entropy model of refs 18−20 representing the shift in the limit glassy heat capacity with respect to the usual extrapolation from the melt. On the left, the effect on the configurational entropy is shown.

Table 1. Physical Parameters of the Investigated PMMA Samples

sample	P1	P2	P3	P4	P5
M_w (g/mol)	1450	4900	11000	21000	55900
T_g (K)	317	366	391	392	395
$\Delta C_p(T_g)$ (J/gK)	0.37	0.34	0.3	0.29	0.28

Some additional hypotheses are necessary to provide the function $C_p^{lim}(T)$. To add only one adjustable parameter, it was introduced the phenomenological shift δ of the $C_p^{lim}(T)$ with respect to $C_p^{liq}(T)$, in a narrow temperature range around the glass-transition temperature, as sketched in Figure 1.

In this paper, we performed DSC experiments in five PMMA samples of different molecular weight, systematically comparing the experimental data with the predictions of both the standard AGV model and the entropic approach. In the following, the latter will be referred to as the Gómez Ribelles model (GR model). Our main interest is devoted to test the power of the AGV model as the molecular weight of the samples is increased and to observe a possible molecular-weight dependence for the additional parameter δ introduced by the GR model.

3. Experimental Section

The PMMA samples were purchased from LabService Analytica and used as received without any further purification. Five different syntheses were used. All of them were almost monodisperse ($M_w/M_n < 1.1$). The weight-average molecular weights were $M_w = 1450$ g/mol (P1), $M_w = 4900$ g/mol (P2), $M_w = 11\,000$ g/mol (P3), $M_w = 21\,000$ g/mol (P4), and $M_w = 55\,900$ g/mol (P5), whereas the glass-transition temperatures, determined according to the enthalpic definition,[41] are reported in Table 1, together with the heat capacity change at T_g.

The entanglement mass for PMMA, as obtained from literature,[44] ranges in the interval 5.8−10.1 kg/mol, depending on the stereochemical composition.

Differential scanning calorimetry measurements were carried out with a Perkin-Elmer DSC 7, frequently calibrated with indium and zinc standards. Highly pure nitrogen was used as purge gas. All thermal treatments were performed without removing the sample from the DSC instrument. For each polymer, a single sample of about 10 mg was used. In the experiments, the samples were: (i) first maintained at a high temperature ($T \approx T_g + 30$ K) for some minutes to erase any

previous thermal history; (ii) quenched ($Q_c = 40$ K (min)$^{-1}$) to the temperature $T_a < T_g$ and then annealed for the aging period t_a; (iii) quenched to a temperature well below the glass transition and finally reheated at the rate of 10 K (min)$^{-1}$, recording the signal.

After each measurement, a reference trace was recorded following the steps (i) and (iii) to obtain the enthalpy loss due to the previous aging.

Intrinsic cycles (cooling at different rates and heating at a fixed rate) have also been performed.

4. Results

For each PMMA sample, we performed several DSC measurements that were compared with the predictions of the AGV and the GR models. Fitting procedures were carried out both on single scans and simultaneously on six different thermograms. We employed the Nedler–Mead search routine[45] to find the minimum in the square deviation. In the simultaneous fitting, the function was minimized:

$$\sigma_a = \frac{1}{6 \cdot N} \sum_{i=1}^{6} \sum_{j=1}^{N} [w(i)\{C_{p,exp}^{N}(i,j) - C_{p,theory}^{N}(i,j)\}]^2 \quad (13)$$

where the index i runs on the experimental scans, whereas the index j is on the data points of each scan. The weighting factors $w(i)$ were assumed proportional to the inverse of the maximum of the overshooting peaks, with $w(i) = 1$ in the case of the thermogram with the highest peak, so that all the experimental curves assume comparable importance in the fitting. Moreover, because of the correlation among the model parameters,[7] the fitting procedures were carried out for various parameter sets, each of them with a fixed value of T_2.

The results pertinent to the lightest sample, P1, have been published in a previous work,[40] then they are briefly reviewed. It has been found that the AGV model describes the experimental P1 data fairly well. In particular, by the fitting procedures on several different thermograms, very moderate thermal history dependence was observed for the parameters with 15% maximum changes.

Various sets of parameters with different T_2 values provided simultaneous fits with comparable agreement with the experiments. The parameter values for some T_2 settings are reported in Table 2. As an example, Figure 2 shows a series of experiments pertaining to different thermal histories, and the predictions corresponding to the set with $T_2 = 237$ K of table.

In this sample, a preliminary analysis of the relaxation enthalpy data evaluated after aging at different glassy temperatures appeared to be consistent with the extrapolation procedure that is at the basis of the fictive temperature definition.

This was carried out according to the following lines.

As a general procedure in calorimetric experiments, the enthalpy lost on aging a glass for a period of time t_a at a given temperature T_a can be evaluated through the relation:[7,23]

$$\Delta H(T_a,t_a) = \int_{T_x}^{T_y} \{C_p^a(T) - C_p^u(T)\}\, dT \quad (14)$$

In this equation, $C_p^a(T)$ and $C_p^u(T)$ are the heat capacity measured after the annealing and that of the unannealed sample, respectively, whereas T_x and T_y are reference temperatures ($T_x < T_g < T_y$). On the other hand, eq 14 actually provides the expression of the experimental enthalpy difference between the thermal treatments with and without annealing at the starting scan temperature, set at $T_g - 80$ K in this work. From the definition of the fictive temperature and neglecting the smooth temperature dependence of $\Delta C_p(T)$ around the glass-transition temperature, it is easily shown that the ΔH evaluation from eq 14 should be compared with the theoretical prediction:[46]

$$\Delta H^{th}(T_a,t_a) = \Delta C_p(T_g) \cdot (T_f^u(T_g - 80) - T_f^a(T_g - 80)) \quad (15)$$

where T_f^u and T_f^a are the values of the fictive temperatures of the unannealed and the annealed experiment, respectively, evaluated at the starting scan temperature. If the enthalpic definition is assumed[41] for the experimental evaluation of T_g, it is $T_g \approx T_f^u(T_g - 80\ \text{K})$. Moreover, $T_f = T_a$ for a long enough annealing at T_a and the glass at the equilibrium; therefore, if relaxation processes are neglected during the second cooling from T_a to $T_g - 80$ K, it is possible to set $T_f^a(T_g - 80\ \text{K}) = T_a$ in eq 15, leading to eq 7. However if the assumption that no relaxation occurs in the second cooling could not be completely fulfilled (T_a near to T_g), eq 7 provides an approximation by defect of the experimental $\Delta H_\infty(T_a)$.

In Figure 3, these approximated predictions are compared with the experimental $\Delta H(T_a, t_a)$, obtained at two annealing temperatures for the P1 sample. The results appear to be compatible with the fictive temperature concept, as definitely confirmed in Figure 4 by the analysis of the experimental enthalpy relaxation isotherms in terms of eq 15. By inspection, the data are very well described by the AGV model (parameters in Table 2, $T_2 = 237$ K).

To conclude, on the P1 sample, the DSC experiments have also been fitted by using the GR model. However, the search routine provided values of the additional shift parameter δ very near to 0 ($|\delta|/\Delta C_p(T_g) < 1\%$), corresponding to no appreciable improvement in the data fit.

The same analysis was carried out for the P2 sample, having a molecular weight slightly lower than the entanglement mass M_e of PMMA.[44] As in P1, P2 DSC scans were simultaneously reproduced with single sets of parameters. In Figure 5, the best fits obtained by setting $T_2 = 276$ K (other parameters in Table 3) are compared with the experimental curves, and a good agreement between theory and experiments can be appreciated. The same set of parameters also provides a good description of the simple cooling/heating thermograms for different cooling rates as shown in Figure 6. In Figure 5, the dotted lines are the best fits obtained by using the GR model with $T_2 = 276$ K. The AGV and GR predictions are almost indistinguishable, as confirmed via the analysis of the square deviation (eq 13). It is found $\sigma_a = 0.024$ for the AGV model and $\sigma_a = 0.022$ for the GR model. Accordingly, the best fit value of the additional parameter δ was found to be 0.022 J/gK, that is, only about 6% of the overall heat capacity change at the glass transition in this polymer ($\Delta C_p(T_g) = 0.34$ J/gK). Similar results were obtained for different T_2

Table 2. Best Fit Parameters of the AGV Model in P1 for Different T_2 Settings

T_2 (K)	B (kJ/mol)	$-\text{Ln}(A(\text{s}))$	β	σ_a
217	50014	54.7	0.45	0.023
237	35121	47.1	0.41	0.017
257	20277	34.9	0.38	0.021

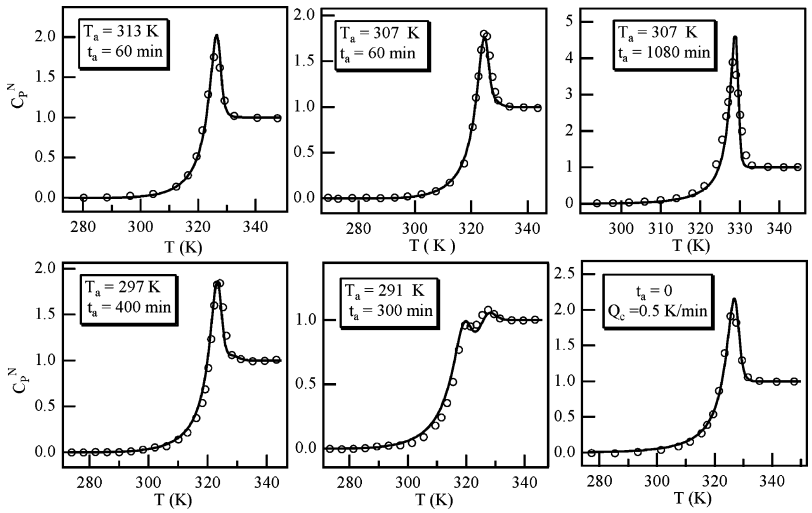

Figure 2. Simultaneous least-squares fit of six different DSC traces of the lowest-molecular-weight PMMA sample (P1) obtained with the AGV model. The thermal histories are reported in the figures (T_a is the aging temperature and t_a is the aging time), whereas the model parameters are in Table 2 ($T_2 = 237$ K). The open circles are the experimental data, and the continuous lines are the fits.

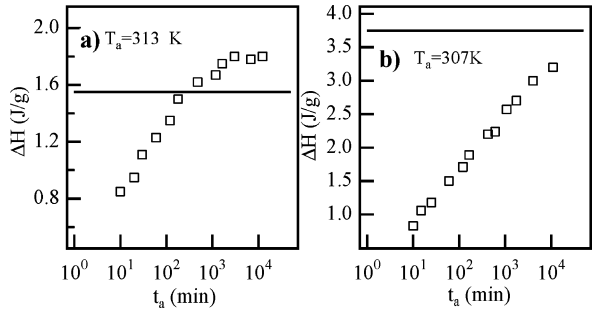

Figure 3. Enthalpy lost on aging the P1 sample (at two different temperatures) as a function of the annealing time (symbols). The lines represent the approximated predictions of the TNM/AGV model obtained with eq 7.

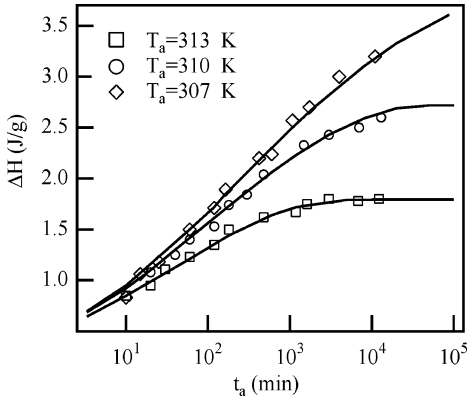

Figure 4. Enthalpy relaxation isotherms recorded after annealing the P1 sample at the three different temperatures in the glassy state reported in the figure. The symbols are the experimental data, whereas the lines are the predictions of the AGV model by means of eq 15 (parameters in Table 2, $T_2 = 237$ K).

settings. Finally, in Figure 7 , we report the relaxational isotherms at two different aging temperatures. The horizontal lines correspond to the approximated asymptotic values obtained from eq 7, whereas the predictions of the AGV and GR models for the setting $T_2 = 296$ K are also reported. By inspection, both the models show similar agreement with experimental data.

Quite different results were found for the P3 sample. In Figure 8, we report six experimental DSC traces and their best simultaneous fit obtained, for $T_2 = 291$ K, with the AGV model (dotted lines) and the GR approach (continuous lines). The thermal histories pertaining to each measurement are reported on the figures. The figure shows an appreciable improvement when the GR model is used. This is confirmed by the average square deviations (eq 13), being $\sigma_a = 0.051$ and $\sigma_a = 0.029$ for the AGV and the GR approaches, respectively. Similar results were found with parameters corresponding to different T_2 settings. In Tables 4 and 5, sets of parameters are reported for the two models. From these tables, it can be immediately understood the reason of the difference in the predictions of the two approaches. In fact, the value of the additional parameter δ amounts to more than 20% of the overall heat capacity change at the glass transition. Because this parameter is related to the long-term behavior of the system, appreciable effects on the enthalpy loss should be detected on aging the sample in the glass for long times. In Figure 9, the results of annealing experiments carried out at $T_a = 387$ K $\approx T_g - 4$ K are reported together with the theoretical predictions of the AGV and GR approaches. Because such predictions depend on the T_2 value,[46] we selected the sets of parameters providing the best agreement at short annealing times. It is apparent from the figure that the AGV model highly overestimates the asymptotic behavior of ΔH, whereas the GR prediction is consistent with the experiments. Interestingly enough, the approximated asymptotic value of ΔH at this temperature from eq 7 (horizontal line in the figure) overestimated the experimental data by about 25%. Therefore, the success of the GR model could have been prophesied a priori. More experiments performed at lower annealing temperatures did not provide further information because of the long relaxation times that prevented $\Delta H(T_a,t_a)$ from behaving in a clear plateau trend.

The studies of the enthalpic relaxation of the two samples, P4 and P5, with the highest molecular weight confirmed the observation carried out in P3. The Figures 10 and 11 show the results of the simultaneous fitting procedures for the AGV and GR model pertaining to these samples. The good performance of the latter is apparent. In Tables 6 and 7, the best fits parameters of the two approaches are reported for different T_2 for the

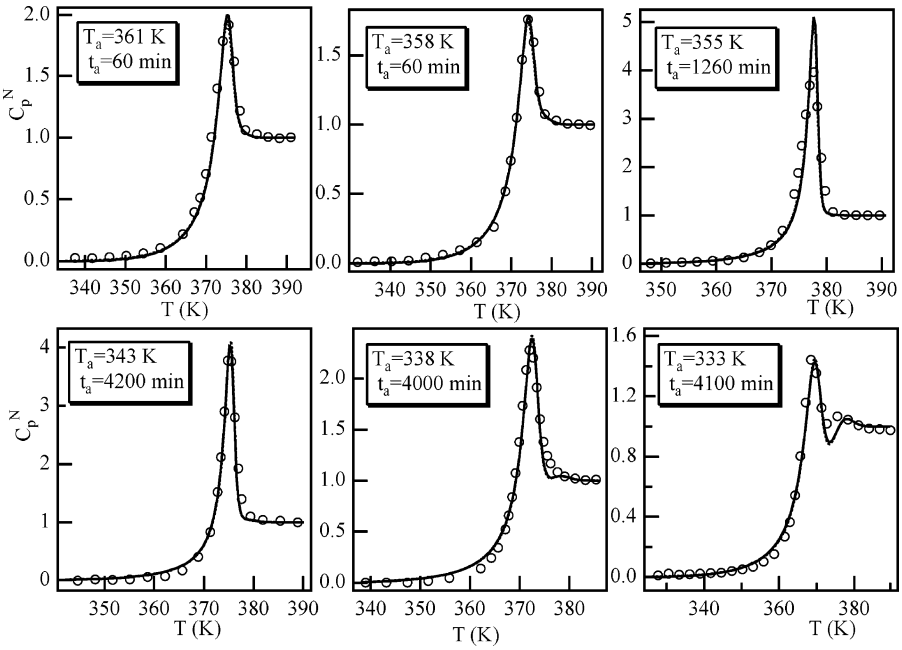

Figure 5. Simultaneous least-squares fit of six different DSC traces of the P2 sample. The continuous lines are the results of the AGV model (parameters in Table 3, $T_2 = 276$ K), whereas the dotted lines refer to the GR model ($-\ln A = 56.5$, $B = 2400$ J/g, $\beta = 0.39$, $\delta = 0.022$, $T_2 = 276$ K). As can be noted, the two predictions are practically indistinguishable.

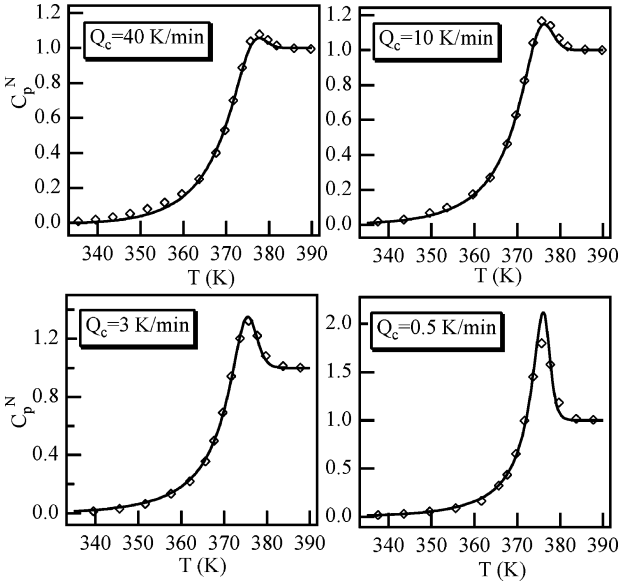

Figure 6. DSC traces recorded after cooling the P2 sample with different cooling rates. The heating rate was fixed to 10 K/min. The symbols are experimental data, whereas the lines are the predictions of AGV model with the parameters obtained by the fitting procedure of Figure 5.

Table 3. Best Fit Parameters of the AGV Model in P2 for Different Fixed Values of T_2

T_2 (K)	B (kJ/mol)	$-$Ln(A(s))	β	σ_a
276	47800	57.6	0.40	0.024
296	33000	49.6	0.36	0.030
315	19300	38.3	0.32	0.042

P4 sample, whereas Tables 8 and 9 refer to P5. Regarding the results reported in Figure 10, obtained with $T_2 = 282$ K, the values $\sigma_a = 0.034$ for the AGV model and $\sigma_a = 0.014$ for the GR approach support on a statistical basis the previous qualitative analysis. In Table 7, it can be observed that the δ parameter shows a stronger T_2 dependence than in the previous sample. Moreover, its mean value obtained from the different parameter

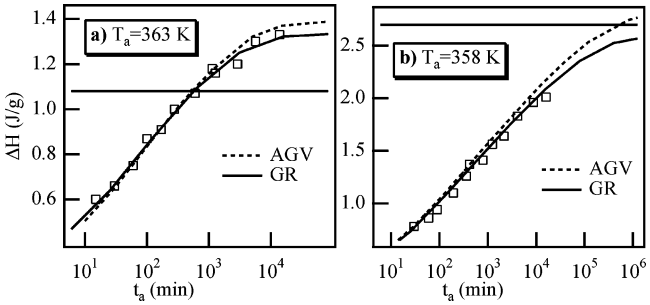

Figure 7. Enthalpy relaxation isotherms recorded on aging the P2 sample at the two temperatures indicated in the figure. The symbols are the experimental data, the horizontal lines are the approximated predictions of eq 7, whereas the continuous and dotted lines are the predictions of the GR and AGV model, respectively (for the AGV model parameters in Table 3, $T_2 = 296$ K; for GR model $-\ln A = 48.4$, $B = 1550$ J/g, $\beta = 0.36$, $\delta = 0.024$, $T_2 = 296$ K).

sets represents about 30% of the overall P4 heat capacity change at the glass transition. Consequently, in this sample, the limit and the extrapolated state should be even more different, with effects that should be easily highlighted through long-time annealing experiments. In Figure 12a, the behavior of the enthalpy lost on aging the P4 sample at $T_a = 388$ K $= T_g - 4$ K as a function of the annealing time is shown. The experimental data are compared with the theoretical predictions of the GR model for two different sets of parameters. It can be noted that all the measurements are bounded by the two theoretical curves. In particular, the obtained values $\Delta H_\infty^{GR}(T_2 = 322\ \text{K}) = 0.86$ J/gK and ΔH_∞^{GR} ($T_2 = 342$ K) $= 0.71$ J/gK have to be compared with the experimental result $\Delta H_\infty^{exp}(388\ \text{K}) = 0.75$ J/gK from averaging the data with $t_a > 1000$ min. Figure 12b shows that very different results were obtained by adopting the AGV model whose predictions highly overestimate the experimental data at long times.

The average value of the shift parameter δ also in the case of the P5 sample is found at a value representing about 30% of $\Delta C_p(T_g)$ (the last column of Table 9).

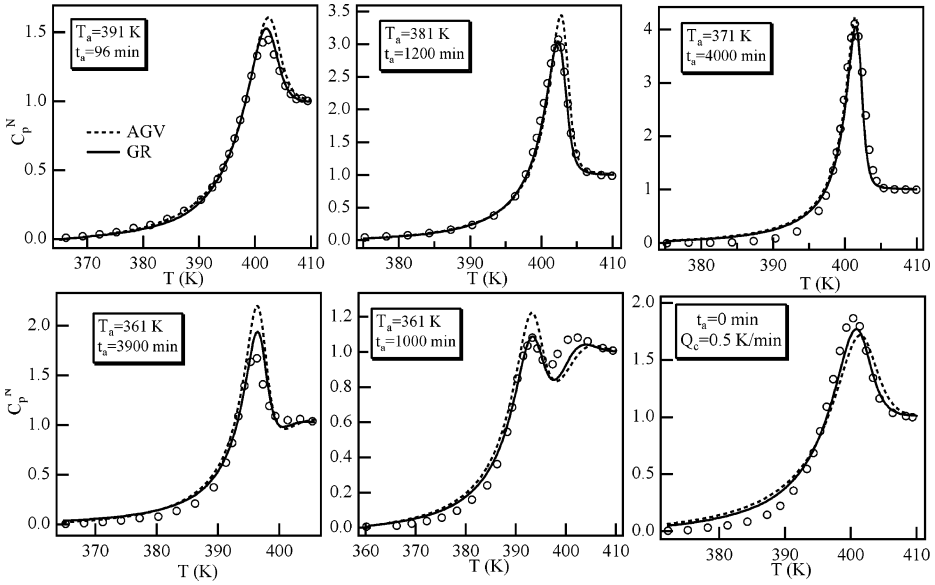

Figure 8. Simultaneous least-squares fit of six different DSC traces of the P3 sample. The dotted lines are the predictions of the AGV model (parameters in Table 4, $T_2 = 291$ K), whereas the continuous lines refer to the GR model (parameters in Table 5, $T_2 = 291$ K).

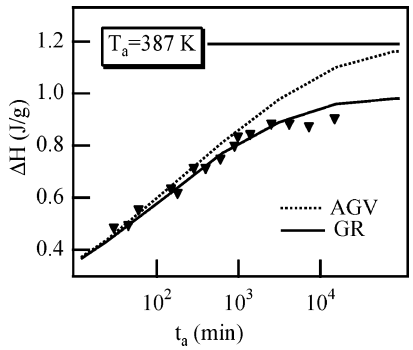

Figure 9. Enthalpy lost on aging the P3 sample at 387 K as a function of the annealing time. The horizontal line represents the approximated prediction of eq 7, whereas the dotted and continuous lines are the predictions of the AGV and the GR model, respectively. The parameters are reported in Table 4 for the AGV approach ($T_2 = 331$ K), and in Table 5 for the GR one ($T_2 = 331$ K).

Table 4. Best Fit Parameters of the AGV Model in P3 for Different T_2 Settings

T_2 (K)	B (kJ/mol)	$-\mathrm{Ln}(A(\mathrm{s}))$	β	σ_a
291	49150	53.3	0.35	0.051
311	33740	44.6	0.32	0.064
331	21290	35.9	0.30	0.081

Table 5. Best Fit Parameters of the GR Entropic Model in P3 for Different T_2 Settings

T_2 (K)	B (J/g)	$-\mathrm{Ln}(A(\mathrm{s}))$	β	δ (J/gK)	σ_a
291	2460	55.5	0.36	0.067	0.029
311	1610	47.2	0.33	0.065	0.037
331	950	37.9	0.31	0.065	0.049

Large differences between the limit state of structural relaxation and the melt-extrapolated state should be expected also in this case. In Figure 13, the experimental values of the enthalpy lost on aging P5 at about 4 K below the glass transition are reported as a function of the annealing times. The data are compared with the predictions of the AGV and GR approaches for the T_2 value, providing the best agreement at short times. Even if less conclusively than in the P4 sample because a clear plateau is not observed, it can be seen that also in this case the predictions of the AGV model largely overestimate the long annealing time behavior of $\Delta H(T_a,t_a)$.

5. Discussion

The present work is devoted to the predictive power of the AGV and GR models for a polymeric material with a known polydispersity index and molecular weight extending beyond the entanglement mass.

The underlying idea is to check the suitability of the models based on TNM formalism in describing the structural relaxation of polymeric systems. These latter models were developed to account for the structural relaxation behavior in inorganic glasses and, consequently, may neglect the peculiar nature of polymers and their dynamics, for example, the presence of topological constraints in high-molecular-weight polymers.

The recent formalism developed in the GR model could be, therefore, more appropriate because it allows for phenomena where a breakdown of the configurational rearrangement can occur and freeze the enthalpic relaxation in a metastable state, intermediate between the initial and completely relaxed one.

The results obtained in this work show that, for the two lowest-molecular-weight PMMA samples, both the AGV and GR model are able to describe the physical aging mechanism fairly well. In particular, different thermal histories are accurately reproduced with single sets of parameters, and importantly enough, the parameter sets obtained with the GR model provide virtually negligible values of the additional δ parameter. These results were also supported by the experimental enthalpy relaxation isotherms, being in agreement with the extrapolation procedure on which the fictive temperature definition rests. Very different results were obtained for the other three samples whose molecular weight was higher than the entanglements mass of PMMA. In fact, greater discrepancies were observed in simultaneous fitting of different DSC curves with the AGV model, and at the same time, the enthalpy lost on aging the samples for long times in the glass was highly overestimated by the theoretical predictions. These results are in fair agreement with the findings of

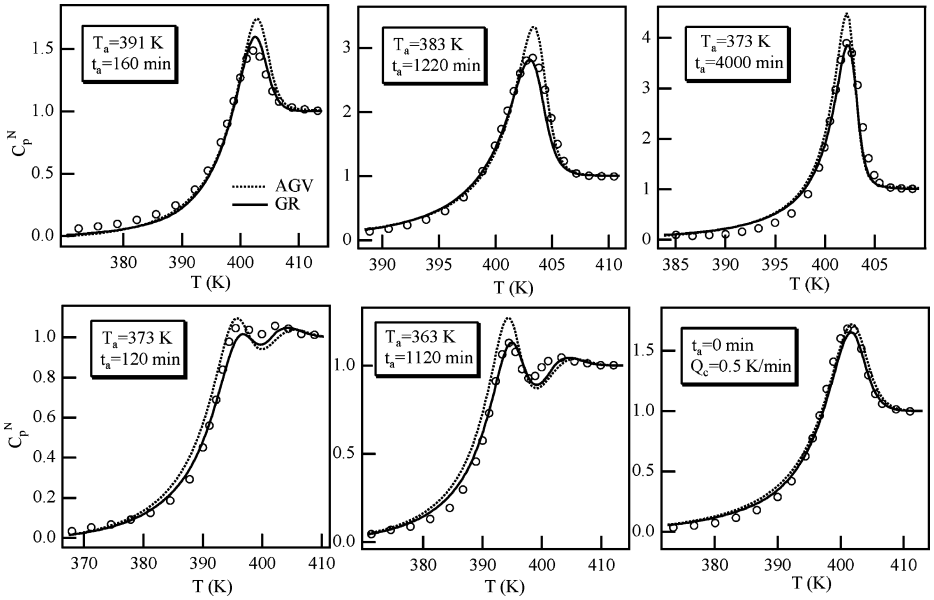

Figure 10. Simultaneous least-squares fit of six different DSC traces of the P4 sample. The dotted lines are the best fits of the AGV model (parameters in Table 6, $T_2 = 282$ K), whereas the continuous lines refer to the GR model (parameters in Table 7, $T_2 = 282$ K). It is apparent the improvement is due to the use of GR model.

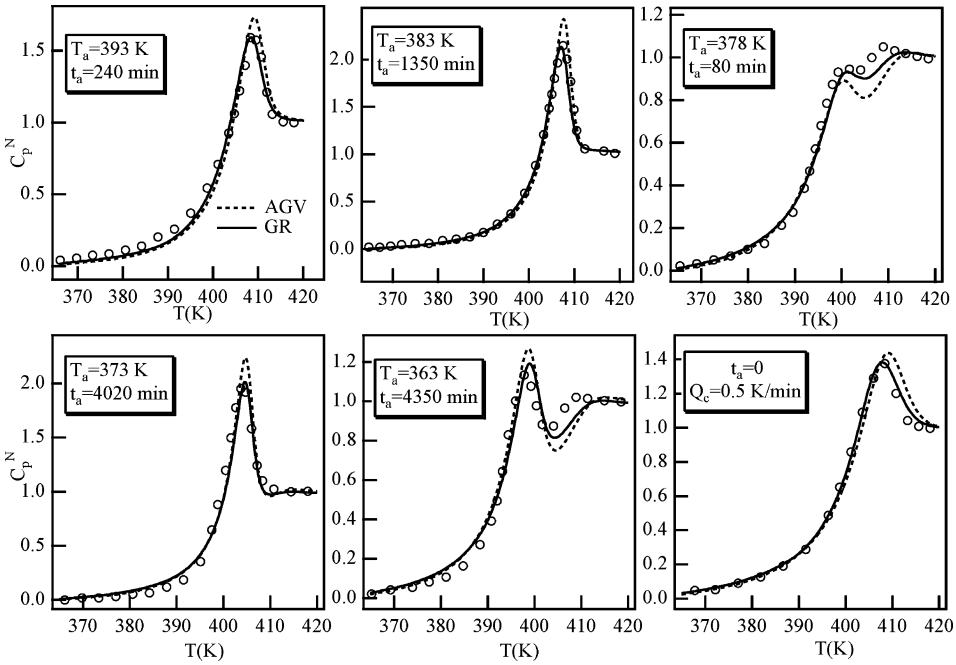

Figure 11. Simultaneous least-squares fit of six different DSC traces of the P5 sample. The dotted lines are the best fits of the AGV model (parameters in Table 8, $T_2 = 284$ K), whereas the continuous lines refer to the GR model (parameters in Table 9, $T_2 = 284$ K).

Table 6. Best Fit Parameters of the AGV Model in P4 for Different Choices of T_2

T_2 (K)	B (kJ/mol)	−Ln(A(s))	β	σ_a
282	58770	58.8	0.36	0.034
302	42830	51.4	0.34	0.042
322	27800	41.6	0.31	0.051
342	15450	30.6	0.29	0.064

Table 7. Best Fit Parameters of the GR Model in P4 for Different Fixed Values of T_2

T_2 (K)	B (J/g)	−Ln(A(s))	β	δ (J/gK)	σ_a
282	2970	60.2	0.37	0.076	0.014
302	2020	52.5	0.35	0.085	0.016
322	1250	43.5	0.32	0.091	0.020
342	660	32.5	0.30	0.094	0.027

previous works investigating the enthalpy relaxation mechanism of high PMMA.[11,12] On the other hand, an appreciable improvement was found by adopting the GR model. The additional parameter of such a model, as referred to the heat capacity change at the glass transition, was found to increase with the molecular weight of the samples ranging from about 20% for the P3 sample to about 30% for last two samples. The observed trend appears to be in agreement with the value $\delta = 0.1$ J/g found in ref 47 for a PMMA synthesis of higher molecular weight.

The improvement in the fit ability of the GR model is connected not only to the addition of a free parameter, but is probably related to its capability to address a crucial flaw of the TNM/AGV formalism, as supported by considering the GR outcomes for the enthalpy loss

Table 8. Best Fit Parameters of the AGV Model in P5 for Different T_2 Settings

T_2 (K)	B (kJ/mol)	−Ln(A(s))	β	σ_a
284	58790	56.3	0.31	0.029
304	41990	47.7	0.28	0.038
324	27270	38.0	0.26	0.050
344	15350	27.6	0.24	0.063

Table 9. Best Fit Parameters of the GR Model in P3 for Different T_2 Settings

T_2 (K)	B (J/g)	−Ln(A(s))	β	δ (J/gK)	σ_a
284	2070	50.0	0.28	0.075	0.012
304	1450	43.3	0.26	0.080	0.014
324	920	35.2	0.25	0.085	0.018
344	500	28.0	0.23	0.091	0.022

on aging at long times in Figures 9, 12, and 13. More importantly, this topic was carefully checked for the P4 sample by comparing the GR predictions with some phenomenological extension of the AGV or TNM models, where the treatment of nonlinearity was handled by adding a free parameter.[17] All of these approaches provided small improvements with respect to the thermograms calculated with the AGV/TNM model, showing a limited predictive power compared to that of the GR model.

The results of the present study support the idea that topological constraints, arising in the polymeric dynamics as the molecular mass increases, play a role in the failure of AGV/TNM model in describing structural relaxation in high polymers. This can be better appreciated in Figure 14, where the behavior of $\delta/\Delta C_p(T_g)$ as a function of molecular weight is shown. By inspection, the sharp change of $\delta/\Delta C_p(T_g)$ at the entanglement mass of PMMA is apparent.[44]

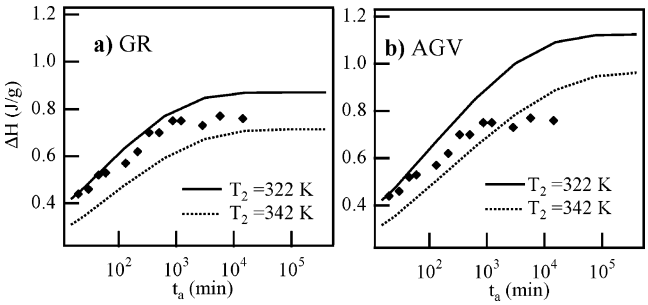

Figure 12. Enthalpy lost on aging the P4 sample at 388 K as a function of the annealing time. The symbols are the experimental data, whereas the dotted and continuous lines represent theoretical predictions obtained for different T_2 settings. Figure 12a refers to the predictions of GR model, whereas Figure 12b concerns the results of the AGV model. The T_2 values are reported in the figures, whereas the other parameters are in the Tables 6 and 7.

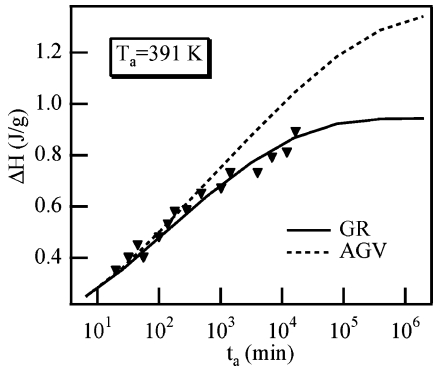

Figure 13. Enthalpy lost on aging the P5 sample at 391 K as a function of the annealing time. The dotted and continuous lines are the predictions of the AGV (T_2 = 344 K and other parameter in Table 8) and GR (T_2 = 344 K and other parameter in Table 9) model, respectively.

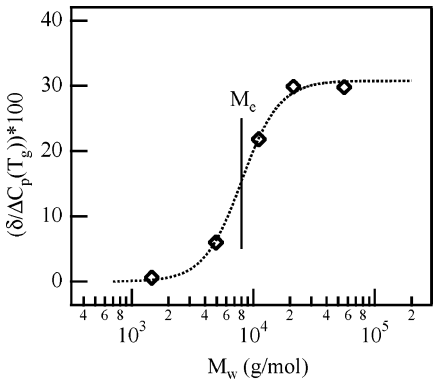

Figure 14. $\delta/\Delta C_p(T_g)$ as a function of the molecular weight. The values of δ were obtained by averaging the values provided by the fitting procedures for the different T_2 settings. The dotted line is an eye guide.

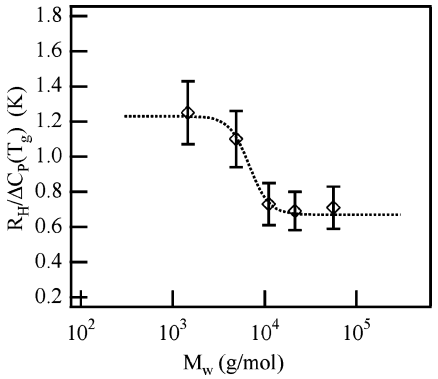

Figure 15. Enthalpy relaxation rate (divided by the heat capacity change at the glass transition) as a function of the molecular weight for the PMMA samples of this study. For all of them, we selected $T_g - T_a \approx 4$ K. The line is an eye guide.

There have been few studies investigating the molecular-weight dependence of enthalpy relaxation in polymers. Several years ago,[48] a comparison was reported on the behavior of different molecular weight polystyrene (PS) samples in terms of their enthalpy relaxation rates R_H, defined as the inflectional slope of the curves of $\Delta H(T_a,t_a)$ vs $\log(t_a)$. The data, conveniently replotted in more recent times,[49] evidenced a steplike behavior with onset near to the entanglement mass of PS.[44] The series of the PMMA polymers investigated in this study shows a comparable behavior (see Figure 15).

In ref 50, the enthalpy relaxation mechanism of some different molecular weight polystyrene samples was also investigated. The TNM model was adopted and the molecular-weight dependence of the model parameters was studied.

The calculated behavior of R_H seems not to contradict the results of ref 48. However, in that work, the parameters were obtained by averaging the values found in fitting single DSC traces. Consequently, the extent of the ability of the model to simultaneously reproduce different experiments is not known. Furthermore, only simple cooling/heating experiments were considered, whereas much more complex thermal histories are necessary to confidently test models of structural relaxation.

A recent work[51] has studied the predictions of the GR model in DSC experiments on five nearly monodisperse

polystyrene samples, nevertheless, without taking into account also the TNM/AGV approach. At variance with the findings of the present work on PMMA, no molecular-weight dependence for the δ parameter ($\delta \approx 0.06$ J/gK) was observed. However, in that study, only one sample had a molecular weight lower than that of the entanglements mass, in practice suggesting the presence of a δ value saturation at high masses. Moreover, the objective function minimized in the fitting routines[52] of ref 51 was slightly different from the one considered in this work, possibly leading to different sets of parameters in correspondence of quite similar calculated thermograms. On the other hand, the values of the parameters obtained from fitting, including the shift parameter δ, were not tested a posteriori by analyzing the enthalpy relaxation isotherms at long times. This has been done in the present work, where this procedure clearly evidenced the consistency of the obtained results. In this respect, it is worth noting that the value of the enthalpy lost on aging a glass is related to the area enclosed below two DSC curves and not to the shape of such curves that can be slightly broadened by thermal lag problems. So, it could be very interesting to perform long-time annealing procedures in the low-molecular-weight sample of ref 51 to check the consistence of the δ value.

Before concluding, a brief analysis of the molecular-weight dependence of the relaxation properties of our PMMA samples is provided. From the GR model parameters, in fact, the temperature dependence of the *equilibrium* structural relaxation times is easily obtained by putting $S_c^{eq}(T)$ in eq 10 instead of S_c. To single out among all the best set of parameters for each sample, a recent experimental protocol was adopted.[46] In Figure 16, the *equilibrium* relaxation times τ are reported as a function of the reduced temperature T_g/T in a narrow range around T_g for the five samples investigated. For the sake of clarity, the glass-transition temperatures were slightly shifted and set in correspondence to a relaxation time of 100 s at $T = T_g$ for all the samples. Looking at the figure, it can be noted that the lightest sample behaves in a quite different manner with respect to the others. A quantitative analysis can be carried out by invoking the fragility concept,[53] which refers to the specific tendency of a liquid to vitrification. The steepness index m[53]

$$m = \left.\frac{\mathrm{d}\log\tau}{\mathrm{d}(T_g/T)}\right|_{T_g} \tag{16}$$

was used as a measure of the dynamic fragility. The obtained results are reported in Figure 17. Note that the m value referring to the sample with the lowest mass is in the range expected for monomers and/or oligomers[54] and for most of van der Waals liquids.[55] By inspection of Figure 17, it can be noted the sharp increase of fragility as the molecular weight increases**.** This finding is in agreement with the results reported in ref 54 **(**see Figure 7 of ref 54**).** A significant increase in fragility with an increase of the molecular weight was also observed for polystyrene (PS).[56] On the contrary, for a homologous series of poly(dimethylsiloxane) (PDMS), the molecular weight had relatively small effects on the fragility.[57] These differences could be ascribed to the different stiffness of the polymeric chains[58] because the more flexible chains of PDMS should realize less benefit from the excess mobility conferred by free ends.

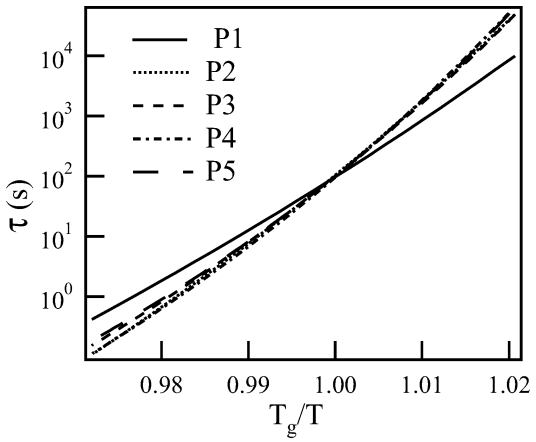

Figure 16. *Equilibrium* structural relaxation times of the PMMA samples, as obtained from the modeling of the enthalpy recovery. The data are plotted as a function of the reduced temperature in a small interval around T_g. For each sample, a unique set of model parameters was singled out by adopting the experimental strategy reported in ref 46.

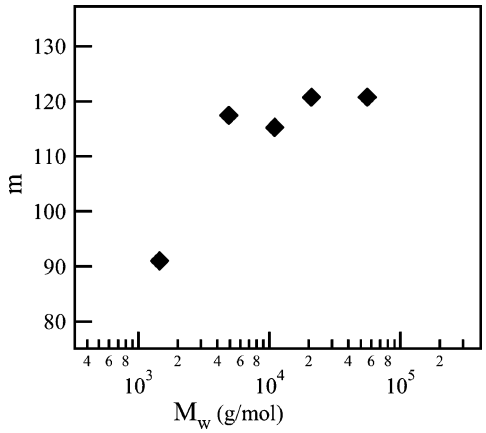

Figure 17. Molecular weight dependence of the dynamic fragility m defined in eq 16, obtained by the curves of Figure 16.

In the last years, the dynamic fragility has been shown to correlate with the chemical structure of polymers,[59] the short time diffusional properties of supercooled liquids,[60] the vibrational motions in polymers,[61] and other basic aspects of glass-former physics.[54,55] In particular, one of the more intriguing correlations concerns the shape of the relaxation function. In fact, it has been demonstrated for a large number of glass-forming liquids that the Kohlrausch parameter β (see eq 1), describing the degree of nonexponentiality of relaxation, decreases with increasing the fragility m.[59,62] These findings are in agreement with our results, as can be verified in Figure 18.

Notwithstanding the successful applications of the fragility approach, its correct interpretation remains an open question. In the past few years, attempts to get further insight on the fragility dilemma have been carried out in the framework of the energy landscape model.[63] Accordingly, the evolution with temperature of the dynamical properties of a glass former is governed by the density of configurational states comprised in its potential energy hypersurface. This idea provides the possibility of connecting the thermodynamic properties with the relaxation mechanisms of glass-forming systems. In fact, because the fragile behavior is associated with the structural instability with respect to the temperature changes, in the framework of the energy

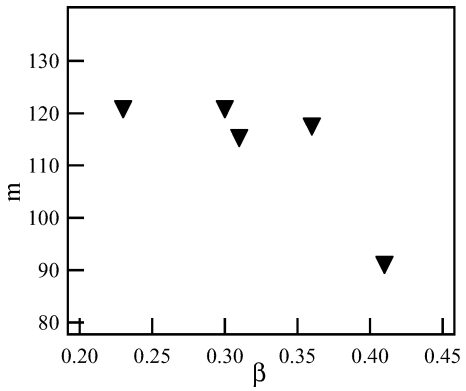

Figure 18. Dynamic fragility as a function of the Kohlrausch β-shape parameter for the investigated PMMA samples. The negative correlation is apparent.

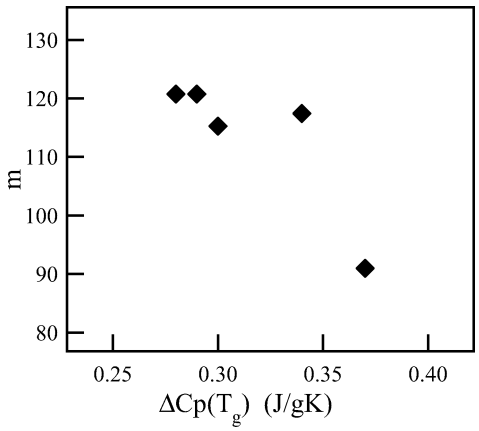

Figure 19. Relationship between dynamic fragility and heat capacity change at the glass transition for the investigated PMMA samples. The observed behavior disagrees with the predictions of the energy landscape model.

landscape picture, it is expected that, when heated through T_g, fragile systems readily make transitions among many configurational states, separated by low energy barriers. This brings us to the prediction of a proportionality between kinetic fragility and the ratio to the barrier height of the configurational heat capacity increment at T_g, $\Delta C_p(T_g)$. A positive correlation between m and $\Delta C_p(T_g)$ was observed for many low-molecular-weight glass formers.[63,64] Moreover, in the last years, for many glass-forming liquids, a positive correlation was demonstrated between kinetic fragility and thermodynamic fragility, the latter defined considering the temperature dependence of configurational entropy.[65] These findings seem to suggest that the sole thermodynamic data could be sufficient to determine the kinetic fragility of a liquid. However, other studies,[55,66] involving larger classes of materials**,** clearly showed that the supposed correlation between kinetic fragility and thermodynamic fragility was not a general rule. In Figure 19, we plot the values of dynamic fragility as a function of $\Delta C_p(T_g)$ for the five PMMA samples investigated in this work. It can be appreciated that there is the presence of a negative correlation already reported in the literature.[55] The results of Figure 19 represent a violation of the prediction of the energy landscape model; because the chemical structure of the systems were unchanged, no variation is expected in the barrier height separating the minima in the energy landscape. Similar conclusions were obtained for other polymeric homologous series.[58,67] Interestingly enough, some recent numerical works devoted to the study of the relationship between potential energy landscape topography and fragility[68,69] have also suggested that thermodynamic data alone are not sufficient for predicting the dynamic fragility. In particular, in ref 68, by starting from elementary basin units containing a single local minimum, different energy landscapes were created sharing identical thermodynamic properties (depth distribution of minima) but drastically different kinetics.

6. Concluding Remarks

In this work, we systematically investigated, through the analysis of differential scanning calorimetry experiments, the physical aging mechanism of PMMA in five almost monodisperse samples with various molecular weights. The data were compared with the predictions of both the standard AGV model and the GR approach. The enthalpy relaxation mechanism of the two lightest samples was described fairly well by both the AGV and GR models. According to the literature, clear discrepancies were found with the AGV model concerning the high-molecular-weight samples, where the GR approach provided appreciable improvements.

The GR model appears able to take into account the presence of topological constraints arising in polymers with molecular mass greater than some critical mass. In particular, the topological information should be concentrated in the additional δ parameter introduced in the GR model. In fact, the δ molecular-weight dependence shows a signature approximately in correspondence with the entanglement mass of PMMA, which clearly suggests that the entanglements play a role in the difference between the equilibrium-extrapolated glassy state and the state attained by the polymer at long times, after which the structural relaxation had taken place. The hypothesis is also validated by the consistency of the δ values with the asymptotic behavior of the enthalpy relaxation isotherms.

More systematic analysis will be required, extending to PMMA samples with even higher molecular weights, to check the possible leveling off of the δ parameter.

This molecular-weight dependence could be, in this case, connected to the similar trends, characterizing different physical properties of the polymeric dynamics such as glass-transition temperature, elastic moduli and compliances, and so on.

Moreover, a more general investigation is needed to gain more insight into the validity of the above findings with respect to the molecular structure of the investigated polymeric materials.

As a final remark, the present study also provided the possibility of investigating the behavior of the dynamic fragility as a function of the polymer mass. At variance with the energy landscape model, a negative correlation was evidenced between such a parameter and the heat capacity change at the glass transition. These results are in agreement with several recent works, suggesting that it is not possible to obtain the dynamic fragility of glass-forming systems starting from thermodynamic data only.

References and Notes

(1) Brawer, S. *Relaxation in Viscous Liquids and Glasses*; American Ceramics Society: New York, 1983.
(2) Narayanaswamy, O. S. *J. Am. Ceram. Soc.* **1971**, *54*, 491−498.
(3) Moynihan, C. T.; Easteal, A. J.; Tran, D. C.; Wilder, J. A.; Donovan, E. P. *J. Am. Ceram. Soc.* **1976**, *59*, 137−140.

(4) DeBolt, M. A.; Easteal, A. J.; Macedo, P. B.; Moynihan, C. T. *J. Am. Ceram. Soc.* **1976**, *59*, 16−21.
(5) Scherer, G. W. *J. Am. Ceram. Soc.* **1984**, *67*, 504−511.
(6) Chow, T. S. *Macromolecules* **1984**, *17*, 2336−2340.
(7) Hodge, I. M. *J. Non-Cryst. Solids* **1994**, *169*, 211−267.
(8) Drozdov, A. D. *Phys. Lett. A* **1999**, *258*, 158−170.
(9) Avramov, I.; Gutzov, I. *J. Non-Cryst. Solids* **2002**, *298*, 67−75.
(10) Lubchenko, V.; Wolynes, P. G. *J. Chem. Phys.* **2004**, *121*, 2852−2865.
(11) Tribone, J. J.; O'Reilly, J. M.; Greener, J. *Macromolecules* **1986**, *19*, 1732−1739.
(12) Cowie, J. M. G.; Ferguson, R. *Polymer* **1993**, *34*, 2135−2141.
(13) Hutchinson, J. M.; Montserrat, S.; Calventus, Y.; Cortés, P. *Macromolecules* **2000**, *33*, 5252−5262.
(14) Cowie, J. M. G.; Harris, S.; McEwen, I. J. *J. Polym. Sci., Part B: Polym. Phys.* **1997**, *35*, 1107−1116.
(15) Brunacci, A.; Cowie, J. M. G.; Ferguson, R.; McEwen, I. J. *Polymer* **1997**, *38*, 865−870.
(16) Andreozzi, L.; Faetti, M.; Giordano, M.; Palazzuoli, D. *Philos. Mag. B* **2002**, *82*, 397−407.
(17) Andreozzi, L.; Faetti, M.; Giordano, M.; Palazzuoli, D.; Zulli, F. *Macromolecules* **2003**, *36*, 7379−7387.
(18) Meseguer Dueñas, J. M.; Garayo, A. V.; Romero Colomer, F.; Estellés, J. M.; Gómez Ribelles, J. L.; Monleón Pradas, M. *J. Polym. Sci., Part B: Polym. Phys.* **1997**, *35*, 2201−2217.
(19) Gómez Ribelles, J. L.; Monleón Pradas, M. *Macromolecules* **1995**, *28*, 5867−5877.
(20) Gómez Ribelles, J. L.; Monleón Pradas, M.; Garayo, A. V.; Romero Colomer, F.; Estellés, J. M.; Meseguer Dueñas, J. M. *Polymer* **1997**, *38*, 963−969.
(21) Doi, M.; Edwards, S. F. *The Theory of Polymer Dynamics*; Oxford University Press: Oxford, 1986.
(22) De Gennes, P. G. *J. Chem. Phys.* **1971**, *55*, 572−581.
(23) Cowie, J. M. G.; Ferguson, R. *Macromolecules* **1989**, *22*, 2307−2312.
(24) Hodge, I. M. *Macromolecules* **1987**, *20*, 2897−2908.
(25) Huang, D.; Yang, Y.; Zhuang, G.; Li, B. *Macromolecules* **1999**, *32*, 6675−6678.
(26) Huang, D.; Yang, Y.; Zhuang, G.; Li, B. *Macromolecules* **2000**, *33*, 461−464.
(27) Chen, J.; Xue, G.; Li, Y.; Wang, L.; Tian, G. *Macromolecules* **2001**, *34*, 1297−1301.
(28) Ferry, J. D. *Viscoelastic Properties of Polymers*; Wiley: New York, 1980.
(29) Tool, A. Q. *J. Am. Ceram. Soc.* **1946**, *29*, 240−253.
(30) Adam, G.; Gibbs, J. H. *J. Phys. Chem.* **1965**, *43*, 139−146.
(31) Hodge, I. M. *J. Res. Natl. Inst. Stand. Technol.* **1997**, *102*, 195−205.
(32) Asami, T.; Matshishi, K.; Onari, S.; Arai, T. *J. Non-Cryst. Solids* **1998**, *226*, 92−98.
(33) Jeong, Y. H.; Moon, I. K. *Phys. Rev. B* **1995**, *52*, 6381−6385.
(34) Hodge, I. M.; O'Reilly, J. M. *J. Phys. Chem. B* **1999**, *103*, 4171−4176.
(35) Cameron, N. R.; Cowie, J. M. G.; Ferguson, R.; McEwan, I. *Polymer* **2001**, *42*, 6991−6997.
(36) Meseguer Dueñas, J. M.; Garayo, A. V.; Romero Colomer, F.; Estellés, J. M.; Gómez Ribelles, J. L.; Monleón Pradas, M. *J. Polym. Sci., Part B: Polym. Phys.* **1997**, *35*, 2201−2217.
(37) Simon, S. L. *Macromolecules* **1997**, *30*, 4056−4063.
(38) Hodge, I. M. *J. Non-Cryst. Solids* **1991**, *131−133*, 435−441.
(39) Mascarell, J. B.; Garcia-Belmonte, G. *J. Chem. Phys.* **2000**, *113*, 4965−4973.
(40) Andreozzi, L.; Faetti, M.; Giordano, M.; Palazzuoli, D. *J. Non-Cryst. Solids* **2003**, *332*, 229−241.
(41) Richardson, M. J.; Savill, N. G. *Polymer* **1975**, *16*, 753−757.
(42) Andreozzi, L.; Faetti, M.; Giordano, M.; Palazzuoli, D. *Macromolecules* **2002**, *35*, 9049−9056.
(43) Kauzmann, W. *Chem. Rev.* **1948**, *43*, 219−256.
(44) Fletters, L. J.; Lohse, D. J.; Graessley, W. W. *J. Polym. Sci., Part B: Polym. Phys.* **1999**, *37*, 1023−1033.
(45) Nedler, J. A.; Mead, R. *Comput. J.* **1965**, *7*, 308.
(46) Andreozzi, L.; Faetti, M.; Giordano, M.; Palazzuoli, D. *J. Phys.: Condens. Matter* **2003**, *15*, S1215−S1226.
(47) Cameron, N. R.; Cowie, J. M. G.; Ferguson, R.; Gómez Ribelles, J. L.; Estelles, J. M. *Eur. Polym. J.* **2002**, *38*, 597−605.
(48) Marshall, A. S.; Petrie, S. E. B. *J. Appl. Phys.* **1975**, *46*, 4223−4229.
(49) Málek, J. *Macromolecules* **1998**, *31*, 8312−8322.
(50) Privalko, V. P.; Demchenko, S. S.; Lipatov, Y. S. *Macromolecules* **1986**, *19*, 901−904.
(51) Sánchez, F. H.; Dueñas, J. M. M.; Gómez Ribelles, J. L. *J. Therm. Anal. Calorim.* **2003**, *72*, 631−640.
(52) Saiter, A.; Oliver, J. M.; Saiter, J. M.; Gómez Ribelles, J. L. *Polymer* **2004**, *45*, 2743−2750.
(53) Böhmer, R.; Angell, C. A. *Phys. Rev. B* **1992**, *45*, 10091−10094.
(54) Ding, Y.; Novikov, V. N.; Sokolov, A. P.; Cailliaux, A.; Dalle-Ferrier, C.; Alba-Simionesco, C.; Frick, B. *Macromolecules* **2004**, *37*, 9264−9272.
(55) Huang, D.; McKenna, G. B. *J. Chem. Phys.* **2001**, *114*, 5621.
(56) Santangelo, P. G.; Roland, C. M. *Macromolecules* **1998**, *31*, 4581−4585.
(57) Roland, C. M.; Ngai, K. L. *Macromolecules* **1996**, *29*, 5747−5750.
(58) Roland, C. M.; Santangelo, P. G.; Ngai, K. L. *J. Chem. Phys.* **1999**, *111*, 5593.
(59) Ngai, K. L.; Roland, C. M. *Macromolecules* **1993**, *26*, 6824−6830.
(60) Roland, C. M.; Ngai, K. L. *J. Chem. Phys.* **1996**, *104*, 2967.
(61) Angell, C. A. *Polymer* **1997**, *38*, 6261.
(62) Bohmer, R.; Ngai, K. L.; Angell, C. A.; Plazek, D. J. *J. Chem. Phys.* **1993**, *99*, 4201.
(63) Angell, C. A. *Science* **1995**, *267*, 1924.
(64) Angell, C. A. *J. Non-Cryst. Solids* **1991**, *131−133*, 13.
(65) Ito, K.; Moynihan, C. T.; Angell, C. A. *Nature (London)* **1999**, *398*, 492.
(66) Ngai, K. L.; Yamamuro, O. *J. Chem. Phys.* **1999**, *111*, 10403.
(67) Santangelo, P. G.; Roland, C. M. *Phys. Rev. B* **1998**, *58*, 14121.
(68) Stillinger, F. H.; Debenedetti, P. G. *J. Chem. Phys.* **2002**, *116*, 3353.
(69) Ruocco, G.; Sciortino, F.; Zamponi, F.; De Michele, C.; Scopigno, T. *J. Chem. Phys.* **2004**, *120*, 10666.

MA0507037